

Biophysical Journal, Volume 96

Supporting Material

Quantitative Modeling and Optimization of Magnetic Tweezers

Jan Lipfert, Xiaomin Hao, and Nynke H. Dekker

Supplementary Material to
Quantitative Modeling and Optimization of Magnetic Tweezers

Jan Lipfert¹, Xiaomin Hao¹, and Nynke H. Dekker^{1,*}

April 2, 2009

¹Kavli Institute of Nanoscience, Faculty of Applied Sciences, Delft University of Technology, Lorentzweg
1, 2628 CJ Delft, The Netherlands

*Corresponding author

Email address of the corresponding author: N.H.Dekker@tudelft.nl

Explicit Form of the Integrals for the Semi-Analytical Calculation of the Magnetic Fields

The principle of the semi-analytical calculations using the Biot-Savart law are explained in the Theory and Experimental Methods section in the main text. Here, we give the explicit form of the integrals that need to be evaluated to compute the magnetic fields for pairs of magnets in the vertical and horizontal geometry. Figure 1B of the main text shows the equivalent current loops for magnet pairs in the two different configurations. We use a coordinate system that is centered between the two magnets (Figure 1) and evaluate the magnetic fields at points along the z-axis. The parameter L denotes the side length of the cubic magnets and g denotes the gap size between the magnets.

Vertical magnet geometry

The contributions of the current segments L1, L3, R1, and R3 (Figure 1B) cancel. For the segments L2, L4, R2, and R4, the \hat{y} and \hat{z} components of the magnetic field cancel each other and only the \hat{x} component of the field remains. The \hat{x} component of the magnet field at a point $(0, 0, z')$ on the z-axis is given by

$$\begin{aligned}
 B_x(0, 0, z') &= \frac{B_r}{4\pi} \left(\int_{L2, R4} \frac{-2(z' - z)}{r^3} dz dy + \int_{L4, R2} \frac{2(z' - z)}{r^3} dz dy \right) \\
 &= \frac{B_r}{4\pi} \left(\int_{-L/2}^{L/2} dz \int_{-L/2}^{L/2} dy \frac{2(z' - z)}{((g/2 + L)^2 + y^2 + (z' - z)^2)^{3/2}} \right. \\
 &\quad \left. - \int_{-L/2}^{L/2} dz \int_{-L/2}^{L/2} dy \frac{2(z' - z)}{((g/2)^2 + y^2 + (z' - z)^2)^{3/2}} \right)
 \end{aligned}$$

Horizontal magnet geometry

Summing over the components L1, L2, L3, L4, R1, R2, R3, and R4, again the \hat{y} and \hat{z} components of the magnetic field cancel and the only non-zero component is along \hat{x} . The \hat{x} component of the magnet field at a point $(0, 0, z')$ on the z-axis for the horizontal magnet configuration is given by

$$\begin{aligned}
 B_x(0, 0, z') &= \frac{B_r}{4\pi} \left(\int_{L2, L4, R2, R4} \frac{2L}{r^3} dx dz + \int_{L1, R1} \frac{2z' + L}{r^3} dx dy + \int_{L3, R3} \frac{-2z' + L}{r^3} dx dy \right) \\
 &= \frac{B_r}{4\pi} \left(\int_{g/2}^{g/2+L} dx \int_{-L/2}^{L/2} dz \frac{2L}{(x^2 + (L/2)^2 + (z' - z)^2)^{3/2}} \right. \\
 &\quad + \int_{g/2}^{g/2+L} dx \int_{-L/2}^{L/2} dy \frac{2z' + L}{(x^2 + y^2 + (z' + L/2)^2)^{3/2}} \\
 &\quad \left. + \int_{g/2}^{g/2+L} dx \int_{-L/2}^{L/2} dy \frac{-2z' + L}{(x^2 + y^2 + (z' - L/2)^2)^{3/2}} \right)
 \end{aligned}$$

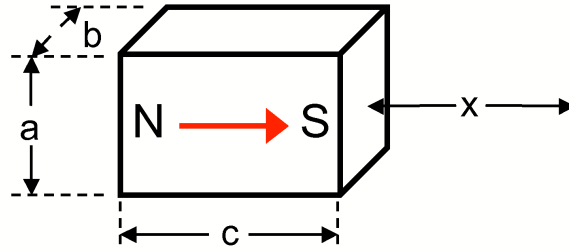
Measurement of the Remanent Field B_r

For a cuboid magnet with dimensions a , b , and c the magnetic field at a distances x along the axis of symmetry of the magnet $B(x)$ (see Supplementary Figure 1) is given by

$$B_x(x) = \frac{B_r}{\pi} \left(\arctan\left(\frac{ab}{2x\sqrt{4x^2 + a^2 + b^2}}\right) - \arctan\left(\frac{ab}{2(c+x)\sqrt{4(c+x)^2 + a^2 + b^2}}\right) \right) \quad (1)$$

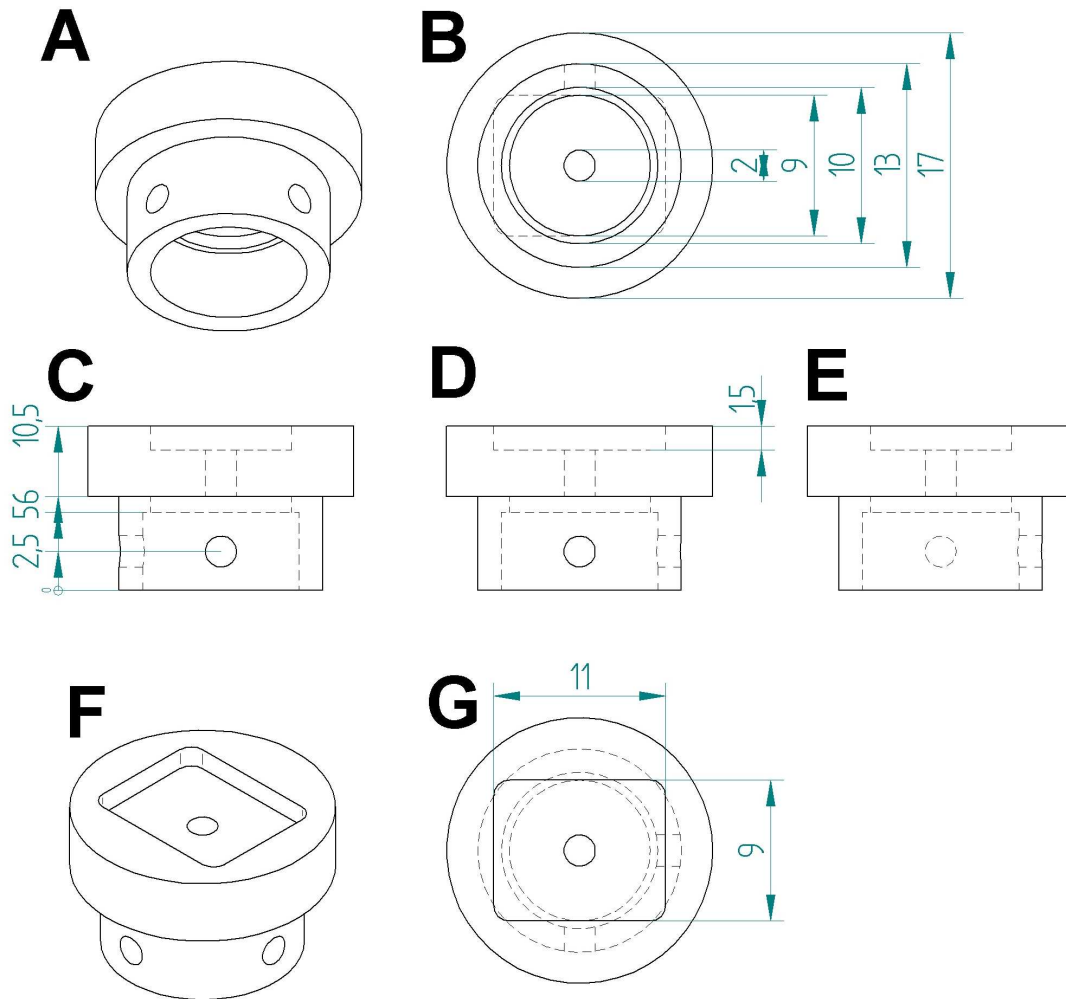
where B_r is the residual magnetic field of the magnet, i.e. the magnetic flux density that remains in the magnet after its initial magnetization (see <http://www.binder-magnetic.fr/?p=e02-e11&cat=18>).

From Eq. 1 B_r can be computed from measurement of the magnetic field close to the magnet's surface. In this work, we use cubic neodymium-iron-boron (NdFeB) permanent magnets (W-05-N50-G, Supermagnete) with $a = b = c = 5$ mm. We measure $B = 0.48 \pm 0.03$ T at $x = 0.3$ mm from the magnets surface, taking into account the thickness of the Hall probe casing, which gives $B_r = 1.24 \pm 0.08$ T.

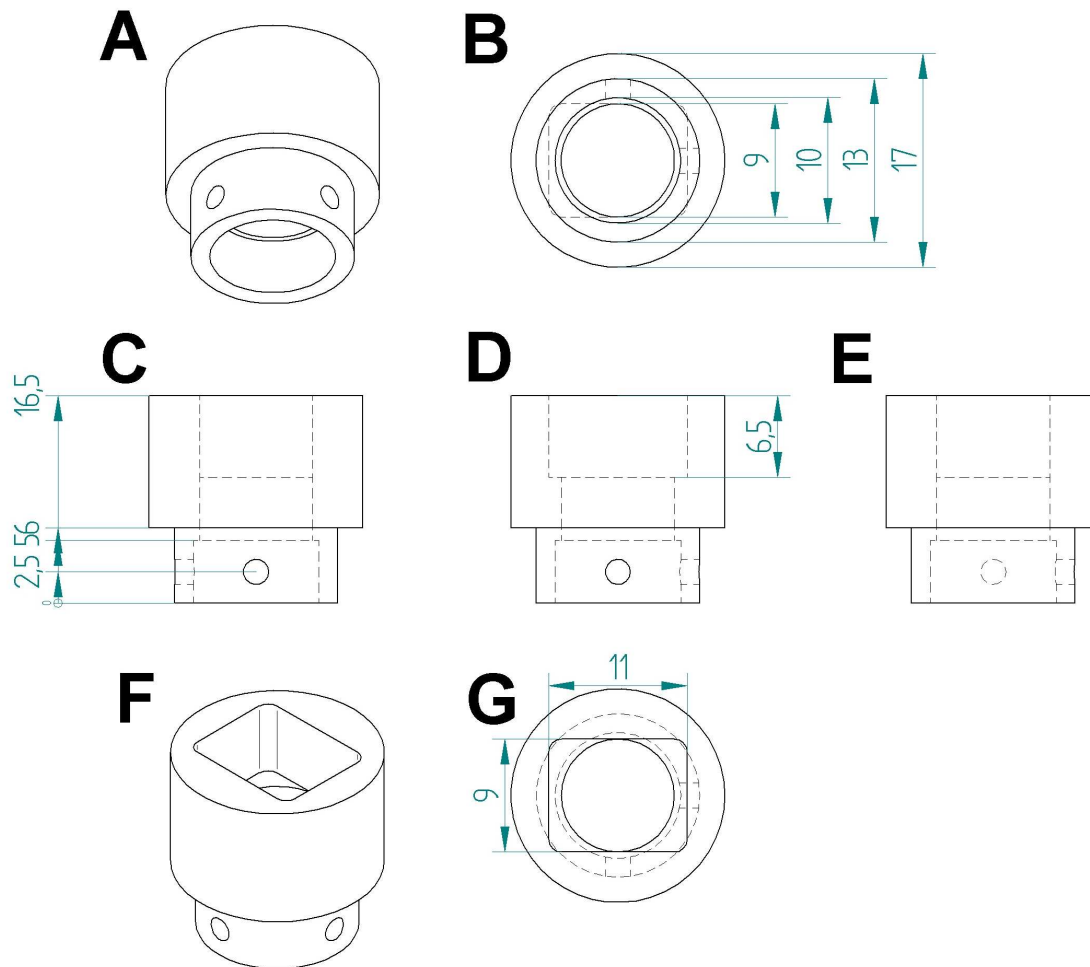


Supplementary Figure 1: Schematic of a cuboid magnet. The magnet dimensions are denoted with a , b , and c . The magnetic field along the axis of symmetry at a distance x is given by Eq. 1.

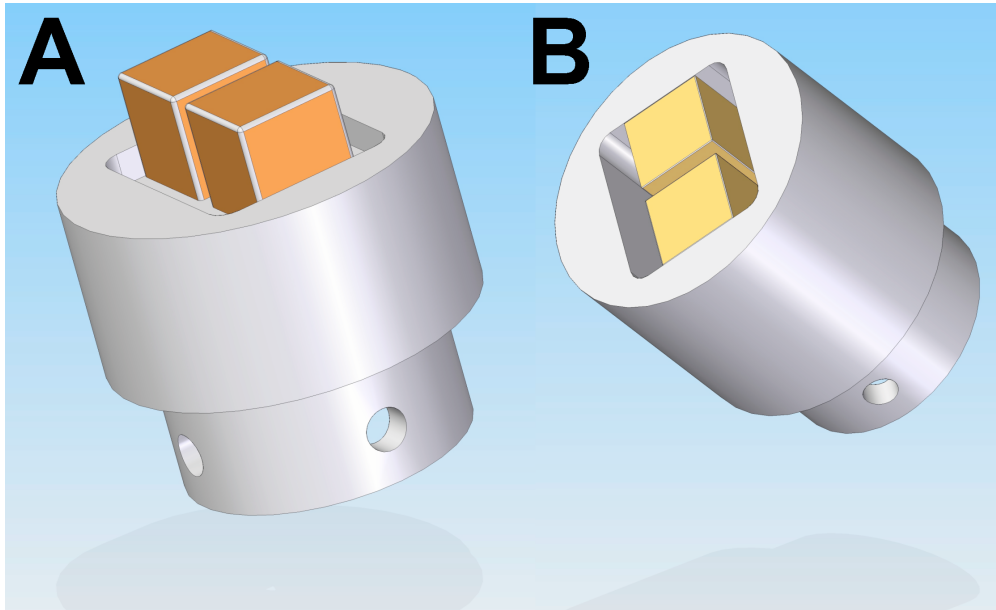
Design Drawings of the Soft Iron Magnet Holders



Supplementary Figure 2: Soft iron magnet holder for magnets in the vertical configuration. Panels A-G show different views of the holder; the indicated dimensions are in mm. The entire piece is machined from soft iron effectively acting as an iron yoke. The presented design is for a gap size of 1 mm using 5 x 5 x 5 mm magnets. Supplementary Figure 4A shows a view with the magnets included.

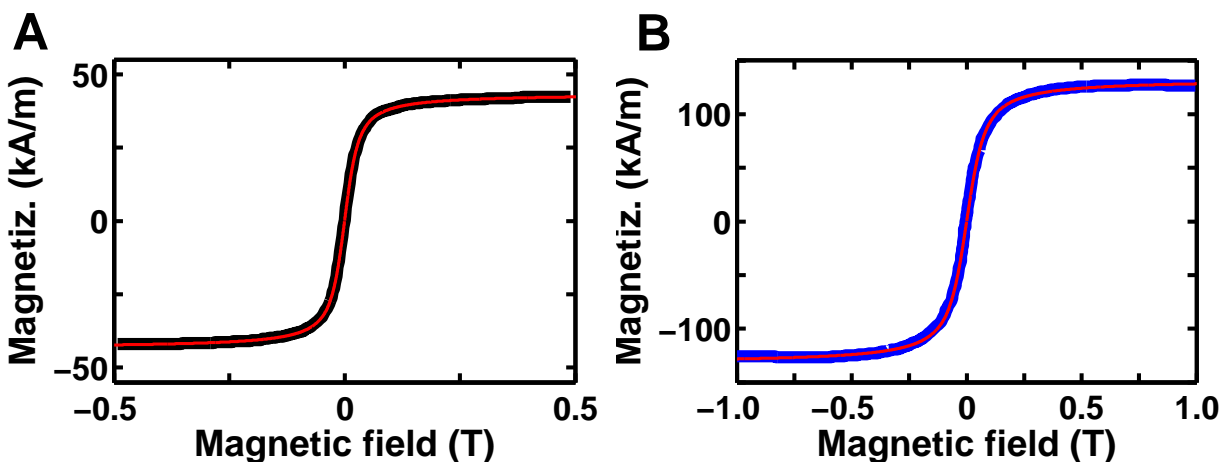


Supplementary Figure 3: Soft iron magnet holder for magnets in the horizontal configuration. Panels A-G show different views of the holder; the indicated dimensions are in mm. The entire piece is machined from soft iron effectively acting as an iron yoke. The presented design is for a gap size of 1 mm using 5 x 5 x 5 mm magnets. Supplementary Figure 4B shows a view with the magnets included.



Supplementary Figure 4: View of the soft iron magnet holders with 5 x 5 x 5 mm magnets included. Magnets are in vertical (A) or horizontal (B) configuration.

Magnetization of MyOne and MagSense Superparamagnetic Beads



Supplementary Figure 5: Volume magnetization of MyOne (A) and 1 μm MagSense (B) beads. The thick black and blue lines are taken from the vendor supplied data, which are obtained by measurements of dried bulk samples using a vibrating sample magnetometer. The red and magenta lines correspond to fits to the data using the Langevin function (see Theory and Experimental Methods).

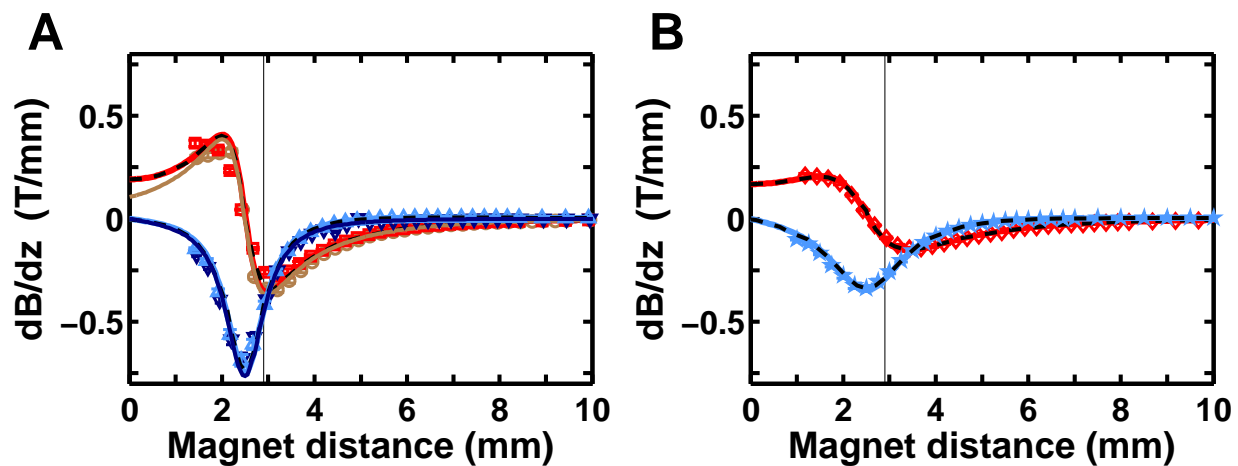
Gravitational Forces on MyOne and MagSense Beads

We estimate the effect of gravitational forces on the beads in our experiments. The gravitational force on the beads is given by

$$F_g = V_b \Delta\rho g \quad (2)$$

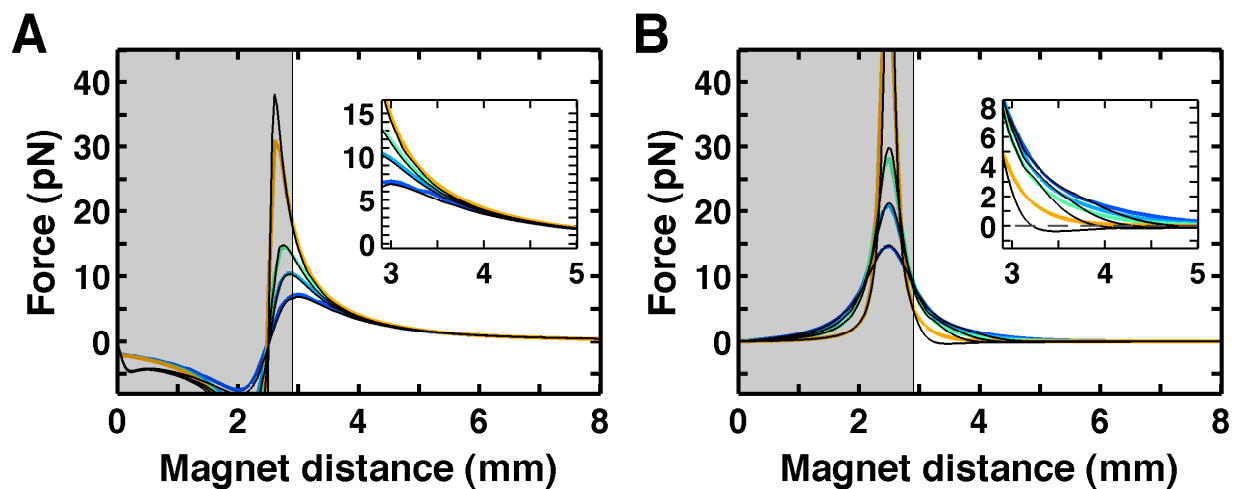
where $\Delta\rho = \rho_{bead} - \rho_{water}$ and g is earth's gravitational acceleration. With $g = 9.81 \text{ m/s}^2$, $\rho_{water} = 1 \text{ g/cm}^3$, and $\rho_{bead} \approx 1.7 \text{ g/cm}^3$ for MyOne beads (1) and 2.5 g/cm^3 for MagSense beads (vendor's specification), we find $F_g \approx 0.003 \text{ pN}$ for MyOne and 0.008 pN for MagSense beads. We neglect this small correction in our analysis.

Magnetic Field Gradients for Pairs of Magnets



Supplementary Figure 6: Magnetic field gradients for pairs of permanent magnets. Magnetic field gradients (in x-direction) as a function of distance from the center of magnet pairs (in z-direction) in the vertical (brown and red) and horizontal (light and dark blue) configuration with a gap size of 1 mm (A) and 2 mm (B). Data points are from measurements with a Hall probe in the absence (red and light blue) and presence (brown and dark blue) of an iron yoke. Solid lines show the results of corresponding calculations using a 3D finite element solver while black dashed lines show the results of semi-analytical calculations (see main text). The thin vertical lines indicate the position of the flow cell surface in our current set-up.

The Effect of the Gap Size on Force in the Presence of an Iron Yoke



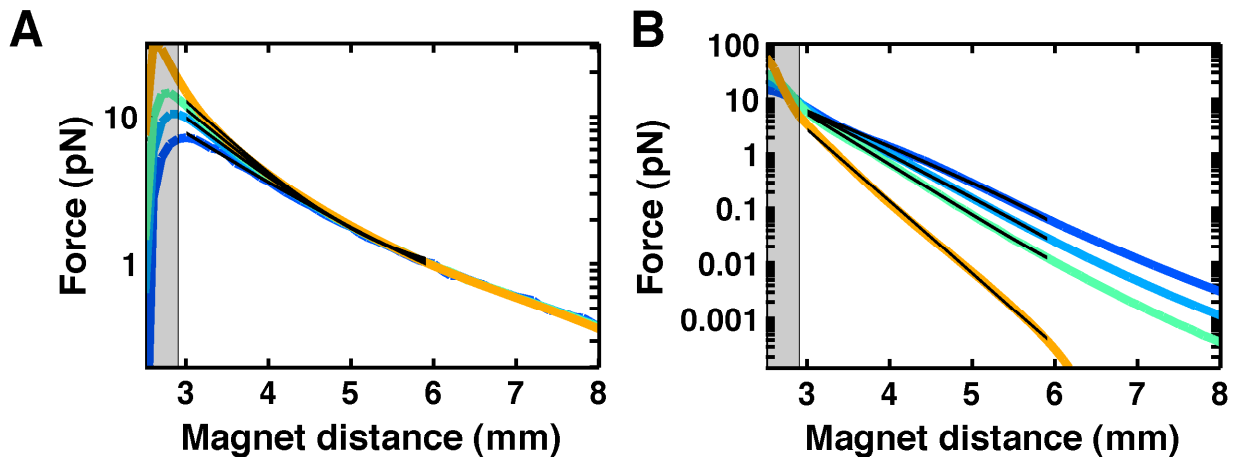
Supplementary Figure 7: The effect of the gap size on force for vertical (A) and horizontal (B) magnet configurations in the presence of an iron yoke. The results of 3D numerical simulations using the parameters for MyOne beads (thick colored lines) are shown for gap sizes of 0.2, 0.5, 0.7, and 1.0 mm (color coded from red to blue, same color code as in Figure 5). For comparison, the corresponding data in the absence of an iron yoke are shown (thin black lines). Insets: Zoom in on the region of closest approach for a 400 μm thick flow cell. The region that is experimentally inaccessible due to the finite thickness of the flow cell is shown as a shaded region in the plots.

Exponential Dependence of the Applied Force on the Distance from the Magnets

In the context of experimental measurements, it can be convenient to have a simple relationship between the distance of the sample from the magnets and the applied stretching force. In previous work (2), an exponential dependence of the form

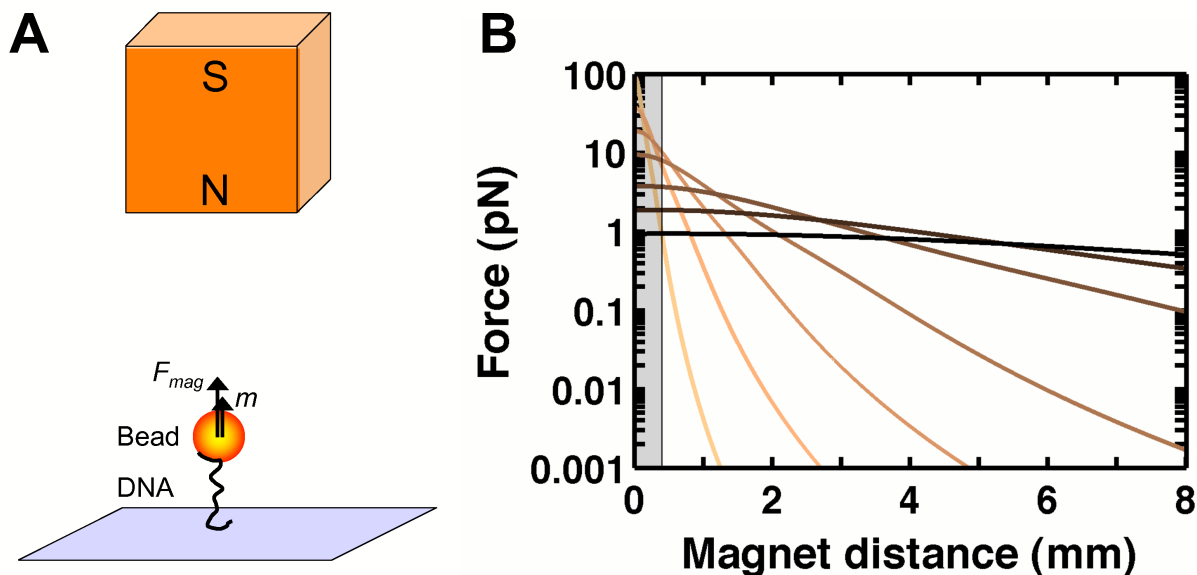
$$F(d) = A \exp(-d/l_d) + F_0 \quad (3)$$

has been used to fit the experimentally measured force data. Here, d is the distance from the magnets' surface and A , l_d , and F_0 are fitting parameters. Having obtained accurate predictions for the stretching forces for different magnet geometries, we can evaluate the validity of the empirical formula Eq. 3. Clearly, Eq. 3 is a poor approximation for the horizontal magnet configuration in the absence of an iron yoke, where the forces change sign. Eq. 3 also fails to take into account the "roll over" of the force observable close to the magnets' surface for the vertical magnet configuration with large g . Bearing in mind these caveats, we find that Eq. 3 does provide a reasonable empirical description for the forces exerted by the horizontal magnet geometry in the presence of an iron yoke and for the vertical magnet geometry with small enough g (Supplementary Figure 3). In these cases the forces can be fit by Eq. 3 with an accuracy of $\leq 10\%$, in particular if the region closest to magnets' surface (< 0.5 mm) is excluded.



Supplementary Figure 8: Exponential dependence of the force on the distance from the magnets. Numerical simulations of forces exerted on MyOne beads for vertical (A) and horizontal (B) magnet geometries for 0.2, 0.5, 0.7, and 1 mm gap size (solid lines, color coded from red to blue). Exponential fits of the form $F(d) = A \exp(-d/l_d) + F_0$ are shown as black lines. d is the distance from the magnets and A , l_d , and F_0 are fitting parameter. The values determined for l_d for 1.0, 0.7, 0.5, and 0.2 mm gap size in horizontal (vertical) geometry are 1.24, 0.99, 0.89, and 0.80 mm (0.67, 0.55, 0.47, and 0.33 mm), respectively. The fitting range is denoted by the length of the black lines. The region that is experimentally inaccessible due to the finite thickness of the magnets and the flow cell (400 μm) is shown as a shaded region in the plot.

Forces from Single Permanent Magnets



Supplementary Figure 9: Forces exerted on beads by a single cubic magnet. A) Schematic of the single magnet set-up in vertical configuration with a tethered bead. B) Stretching forces as a function of the distance from the magnet in vertical configuration for different magnet sizes. Forces were predicted using the semi-analytical model with the parameters for MyOne beads for cubic magnets with 0.2, 0.5, 1, 2, 5, 10, 20 mm side length (color coded from light to dark). The distance is measured from the magnet surface, to aid comparison of the differently sized magnets. The region that is experimentally inaccessible due to the finite thickness of a 400 μm -thick flow cell is shown as a shaded region in the plot. The forces for a single magnet in the horizontal configuration are similar to the forces from a pair of magnets in the horizontal configuration in the limit of small gap size (not shown).

References

1. Fønnum, G., C. Johansson, A. Molteberg, S. Morup, and E. Aksnes, 2005. Characterization of Dynabeads by magnetization measurements and Mössbauer spectroscopy. *J. Magn. Magn. Mat.* 293:41–47.
2. Kruithof, M., F. Chien, M. de Jager, and J. van Noort, 2008. Subpiconewton dynamic force spectroscopy using magnetic tweezers. *Biophys. J.* 94:2343–2348.